

Hole-blocking titanium-oxide/silicon heterojunction and its application to photovoltaics

Sushobhan Avasthi,¹ William E. McClain,^{1,2} Gabriel Man,^{1,3} Antoine Kahn,^{1,3} Jeffrey Schwartz,^{1,2} and James C. Sturm^{1,3}

¹Princeton Institute for the Science and Technology of Materials (PRISM), Princeton University, New Jersey 08544, USA

²Department of Chemistry, Princeton University, New Jersey 08544, USA

³Department of Electrical Engineering, Princeton University, New Jersey 08544, USA

(Received 10 November 2012; accepted 16 April 2013; published online 21 May 2013)

In contrast to the numerous reports on narrow-bandgap heterojunctions on silicon, such as strained $\text{Si}_{1-x}\text{Ge}_x$ on silicon, there have been very few accounts of wide-bandgap semiconducting heterojunctions on silicon. Here, we present a wide-bandgap heterojunction—between titanium oxide and crystalline silicon—where the titanium oxide is deposited via a metal-organic chemical vapor deposition process at substrate temperatures of only 80–100 °C. The deposited films are conformal and smooth at the nanometer scale. Electrically, the TiO_2/Si heterojunction prevents transport of holes while allowing transport of electrons. This selective carrier blocking is used to demonstrate a low-temperature processed silicon solar cell. © 2013 AIP Publishing LLC [<http://dx.doi.org/10.1063/1.4803446>]

The main device advantage of heterojunctions is the ability to selectively block the flow of either electrons (via conduction band barrier) or holes (via valence band barrier). So, heterojunctions can augment, or replace, the traditional p-n junction to achieve similar effects.^{1,2} The primary limitation in fabricating such heterojunctions on crystalline silicon (bandgap $E_g = 1.12$ eV) is the lattice mismatch between silicon and the other semiconductor.² The mismatch is small for the $\text{Si}_{1-x}\text{Ge}_x$ alloys ($E_g = 0.8$ – 1.1 eV), only $\sim 1\%$ for $x = 0.25$, and narrow bandgap heterojunctions can be fabricated on silicon by compressively straining thin SiGe layers to match the silicon lattice.³ However, this pseudomorphic lattice matching is not feasible for making wide bandgap heterojunction on silicon using wideband gap column IV semiconductors, e.g., 3C-SiC ($E_g = 2.4$ eV (Ref. 4)) and diamond ($E_g = 5.4$ eV (Ref. 4)). Though both 3C-SiC and diamond have the same lattice structure as silicon, their lattice constants are 20% and 35% smaller than that of silicon, making the mismatch too large to be compensated by straining thin layers.⁵ An interesting approach to circumvent the problem of lattice mismatch is to consider heterojunctions between crystalline silicon and amorphous semiconductors such as titanium dioxide.

Titanium dioxide has been previously used as an antireflection coating (ARC) in solar cells,⁶ as an alternative to silicon-nitride/silicon-oxide for passivating the Si surface⁷ and as a gate dielectric.⁸ In organic photovoltaics, titanium oxide nanoparticles have been used to aid electron injection.⁹ However, a hole-blocking TiO_2/Si heterojunction on crystalline silicon or its application for silicon photovoltaics has not been reported.

Prior to titanium dioxide deposition, the silicon surface is cleaned using the well known RCA-clean recipe followed by 1 min 1:100 hydrofluoric acid etch to hydrogen-passivate the surface.¹⁰ The titanium dioxide is deposited by a simplified chemical vapor deposition (CVD) process that uses titanium(IV) tetra-(tert-butoxide) as the precursor. A deposition cycle

consists of two steps. First, the silicon (100) wafer is cooled to -10 °C and vapors of the Ti-alkoxide are introduced into the chamber for 5–10 min. This step forms a thin layer of adsorbed Ti-alkoxide on the silicon surface. Second, the silicon wafer is heated (80 to 100 °C) for 5 min to thermolyze the Ti-alkoxide into titanium dioxide. Depending on the length of the cooling (or adsorbing) step, one complete cycle results in the deposition of 1–4 nm of titanium dioxide. Thicker films can be deposited by repeating the deposition cycle multiple times^{11,12} but in the titanium dioxide layers discussed in this paper were all deposited in one cycle. The titanium dioxide deposition system consists of a quartz bulb holding the precursor, a quartz reaction chamber with a base pressure of 50 mTorr, and a pumping system. The silicon samples sit on a copper stage inside the reaction chamber, and the internal temperature is cycled by externally heating and cooling the whole reaction chamber using a heat-tape and dry ice. The sample temperature is estimated by a thermoelectric probe in contact with the chamber. The pumping system consists of a single stage mechanical pump which allows chamber to reach base pressures below 50 mTorr.

The deposition process described above is similar to atomic layer deposition (ALD) in that it is used to deposit nanometer thick layers using an adsorbed precursor;¹³ however, there are two notable differences. First, unlike ALD, the process does not use a second reactant, such as water, to react with the Ti-alkoxide precursor to form titanium dioxide. This simplifies the deposition system, in that no bubblers or high-speed isolation valves are required. Second, unlike ALD precursors, like titanium tetrachloride, titanium(IV) tetra-(tert-butoxide) is not intrinsically self-limiting. This leads to a deposition regime where the thickness of the deposited metal-oxide is a function of adsorption time. Due to the two differences, our deposition process is better described as a modified CVD process.

The thickness of the titanium dioxide layers was measured by ellipsometry in a Gaertner Stokes Ellipsometer LSE.

The system used a 632.8 nm laser at two angles to yield both thickness and refractive index. Measurements were taken at 5–10 different spots on the sample. The titanium dioxide layers discussed in this manuscript were found to be 1–4 nm thick, with a standard deviation of less than 5%. The refractive indices of the deposited films were usually around 2.2–2.7. These values are comparable to the refractive index of titanium dioxide in the rutile phase, 2.8,¹⁴ suggesting that the deposited films are relatively dense.

To confirm the presence of a titanium dioxide layer and to investigate the chemical oxidation state of the titanium atoms, X-ray photoelectron spectroscopy (XPS) was used. For the XPS measurements, titanium dioxide was first deposited on a highly doped p-Si (<0.005 Ω cm). Samples were then transported in air to the measurement system. The XPS measurements were performed in a dedicated UHV chamber with a base pressure of $<2 \times 10^{-10}$ Torr. Al $K\alpha$ radiation at 1486.6 eV was used in XPS, with an experimental resolution of 0.5 eV.

The measured Ti 2p spectrum shows two peaks at binding energies of 459.7 and 465.3 eV (Fig. 1). The peak position of Ti 2p_{3/2} at 459.7 eV compares well to the peak position for Ti 2p_{3/2} for Ti⁴⁺ in TiO₂ (458.6–459.2 eV), and is significantly different from the Ti 2p_{3/2} peak of Ti⁺² (454.9–455.2 eV) and Ti⁰ (453.7–454.2 eV).¹⁵ The intensities of the peak at 459.7 eV and 465.3 eV have a ratio of 2.2:1, close to the branching ratio of 2:1 expected for the 2p lines. Finally, the measured spin-orbit splitting is 5.6 eV, which compares more favorably to the spin-orbit splitting of Ti⁴⁺ (5.5 eV) rather than to the spin-orbit splitting of Ti⁰ (6.2 eV).¹⁵ In summary, the XPS measurements confirm the presence of titanium dioxide on the surface.

To investigate the morphology and texture of the deposited titanium dioxide layers, Atomic force microscopy (AFM) measurements were done on a Dimension Nanoman (Veeco Instruments). AFM reveals an extremely smooth and conformal film with a RMS roughness of only 0.5 nm (image not shown here) over a scan area of 50 $\mu\text{m} \times 50 \mu\text{m}$. No long-range features or cracks are observed anywhere on the surface (sample size is 1.6 cm \times 1.6 cm). Also of interest is

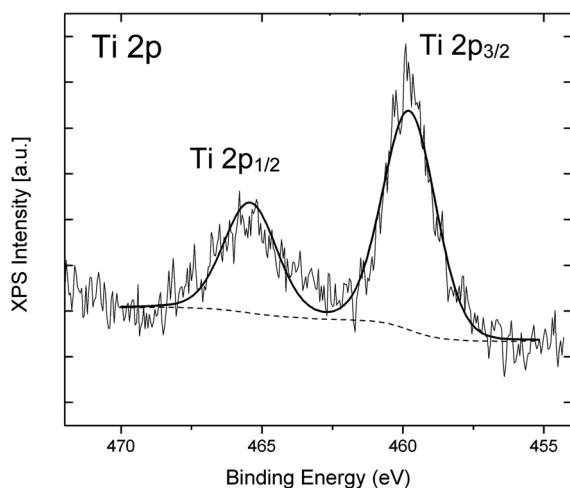


FIG. 1. Ti 2p XPS spectrum of the titanium dioxide layer on silicon. Also shown are the fitted Gaussian peaks (bold line) and the Shirley background (dashed line).

the crystallographic nature of the titanium dioxide film. If present, grain boundaries in a polycrystalline titanium dioxide layer would be visible in the phase image of atomic force microscopy.¹⁶ In the phase image of our film, no grain boundaries are visible (RMS = 0.94°), suggesting that the titanium dioxide layer is amorphous and not polycrystalline. The lack of crystal boundaries is in contrast to previously reported results where the anatase phase has been observed at deposition temperatures above 275 °C.¹⁷ We speculate that the lack of crystallinity in our titanium dioxide layer is due to the much lower deposition temperature (~ 100 °C).

The different forms of titanium dioxide (rutile, anatase, nanoporous, etc.) are all semiconducting with empty and filled band edges at ~ 4.0 eV and 7.0–7.2 eV below the vacuum level, respectively.^{9,18} In comparison, at the Si (100) surface, the conduction band edge (electron affinity) and valence band edge (ionization energy) are at about 4.05 eV and 5.17 eV below the vacuum level, respectively, although these values vary with surface preparation and termination. The TiO₂/silicon interface is, therefore, expected to have a large valence-band (VB) barrier ($\Delta E_V \approx 2.0$ eV), which would block the transport of holes from silicon to titanium dioxide, but a small conduction-band (CB) barrier ($\Delta E_C \approx 0.05$ eV), which would allow transport of electrons from silicon to titanium dioxide (Figs. 2(a) and 2(b)).

To experimentally test the band-offsets at the TiO₂/Si interface, devices were fabricated on p-type and n-type Si wafers coated with a 3 nm thick titanium dioxide layer deposited in a single cycle. For the cathode, a 15 nm thick layer of

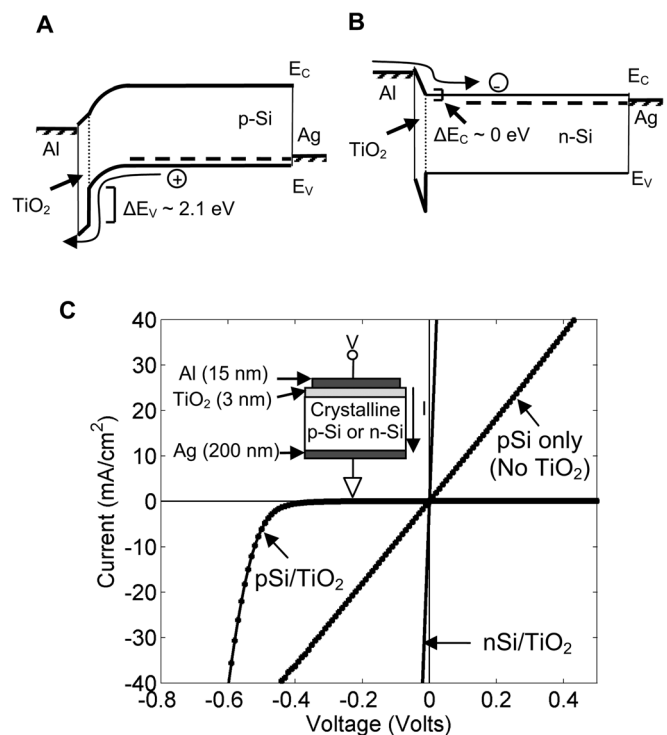


FIG. 2. Band diagrams of the TiO₂/Si heterojunction test diodes on (a) p-Si and (b) n-Si showing the flow of majority carriers in dark under negative-bias on the Al electrode. (c) Dark I-V characteristics of Al/p-Si Schottky diode with and without titanium dioxide. The structure of the device with titanium dioxide is shown in the inset. The voltage is applied to the top electrode and positive current flows from metal to Si. Also shown are the dark I-V characteristics of Al/n-Si Schottky diode with the titanium dioxide layer.

aluminum was deposited on top of the titanium dioxide layer. The cathode was patterned into 1 mm radius circles via a shadow mask (0.03 cm^2). For the anode, a blanket coating of silver was deposited on the backside of the silicon wafers, forming a large-area Ohmic contact (structure and band-diagrams shown in Figs. 2(c) and 2(d)). The metal layers were deposited by a thermal evaporation in an Edwards 306 A deposition system. The metal thickness was measured by an *in-situ* quartz crystal monitor. The current-voltage measurements were taken with an Agilent 4155B parameter analyzer. The bulk resistivity of the titanium dioxide films, extracted from the lateral current between two metal contacts, was greater than $5 \text{ M}\Omega \text{ cm}$. Due to the high lateral resistance, we do not expect much current spreading in the 3 nm thick titanium dioxide layer, so the device area is assumed to be the same as the top contact area, i.e., 0.03 cm^2 .

It is well known that aluminum deposited directly on p-type Si forms a “Schottky” junction with a very low barrier for holes flowing from silicon to aluminum.¹⁹ At room-temperature, the current-voltage characteristics are usually ohmic, i.e., not blocking. If the deposited titanium dioxide layers are indeed hole-blocking, with a valence band edge far below that of silicon and low interface defect-density, then inserting the titanium dioxide between aluminum and silicon would block the flow of holes. This hypothesis was tested by comparing the characteristics of Al/p-Si devices fabricated with and without an intermediate titanium dioxide layer.

Without the titanium dioxide layer, the current-voltage characteristics were indeed Ohmic, due to the small hole-barrier (“pSi/TiO₂” and “pSi only” curves in Fig. 2(c)). On the other hand, devices made with a 3 nm titanium dioxide interlayer visually showed no current for small biases ($< 0.5 \text{ V}$), confirming that the titanium dioxide layer acts as a hole-blocker. The effective blocking of holes in devices with area of 0.03 cm^2 further shows that the titanium dioxide layers are relatively pin-hole free on a millimeter scale.

To investigate the conduction-band offset of the TiO₂/Si interface, similar devices were fabricated on n-type silicon where electrons carry most of the current. The measured characteristics of Al/TiO₂/n-Si show Ohmic characteristics (“nSi/TiO₂” curve in Fig. 2(c)). This indicates that the TiO₂/Si interface does not block electrons and that the conduction band-offset (ΔE_C) is indeed negligible at TiO₂/Si interface. Assuming that the band-offsets at the TiO₂/Si interface do not change with Si doping type, the current-voltage characteristics of Fig. 2(c) qualitatively confirm the band-alignment posited in Figs. 2(a) and 2(b).

One possible application of a single-carrier-blocking, or carrier selective, wide bandgap heterojunction is in photovoltaics, previously demonstrated in the AlGaAs/GaAs material system.²⁰ Not only can such a heterojunction, in principle, provide better photovoltaic performance than a diffused p-n homojunction but the low fabrication temperature of the TiO₂/Si heterojunction ($80\text{--}100^\circ\text{C}$) may also have cost advantages over the diffused p-n junction that is typically fabricated at $\sim 900^\circ\text{C}$.

Very few heterojunctions between wide gap semiconductors and crystalline Si have been realized, primarily because of lack of adequate material and interface. One successful

example is the amorphous-Si/crystalline-Si heterojunction developed by Sanyo²¹ but the technology requires a plasma-enhanced CVD chamber. Organic semiconductors, with bandgaps $\sim 2\text{--}3 \text{ eV}$, have also been demonstrated to form wide-bandgap organic/silicon heterojunctions.²² Most of the organic/silicon heterojunctions cells demonstrated have shown electron-blocking characteristics and not hole-blocking characteristics, although conceptually hole-blocking function could be implemented by choosing appropriate organic materials with low electron affinity and large ionization energy. Here, we demonstrate the application of the hole-blocking TiO₂/Si heterojunction to photovoltaics, using a device which is complementary to the electron-blocking organic/silicon device described in Ref. 22. The solar cell current-voltage characteristics were measured using a HP 4155 parameter analyzer using a two contact setup—one contact for the anode and one for the cathode. An Optical Radiation Company solar simulator was used to measure the AM1.5 response.

The structure of the photovoltaic cell shown in Fig. 3(a) comprises of a 10^{15} cm^{-3} p-type doped silicon (100) wafer

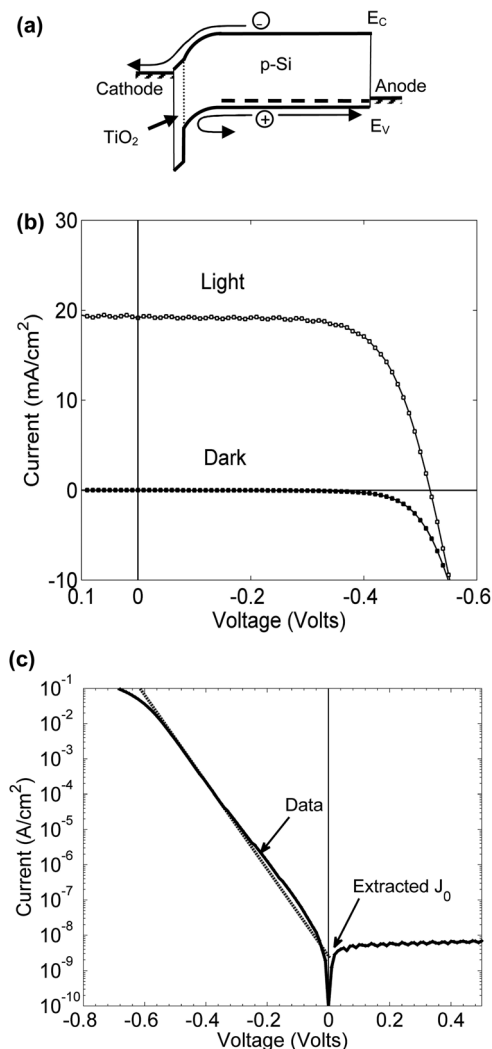


FIG. 3. (a) Band diagrams of the TiO₂/Si heterojunction solar cell showing transport of photogenerated electrons and holes. (b) The I-V characteristics of the TiO₂/Si heterojunction solar cell in dark and under AM 1.5 illumination. The top metal lets in $\sim 50\%$ of the incident light. (c) The I-V characteristics of the TiO₂/Si heterojunction solar cell in dark on a semilog plot to highlight the extracted value of J_0 .

coated with a 4 nm thick layer of titanium dioxide on the top. The top electrode is aluminum, which is deliberately kept very thin (15 ± 5 nm) to allow some light to pass through. To measure the transmission through the semi-transparent aluminum, we deposited the 15 nm aluminum on a glass slide. By comparing the photocurrent of an underlying silicon photodiode, with and without the aluminum coated glass slide, we estimate that the aluminum layer lets in approximately 50% of the light. This is not an optimum transparent electrode for photovoltaics, but given that we need the top electrode with a low-work function for high open-circuit voltage (work function of Al ~ 4.0 eV), a semi-transparent electrode is sufficient for a proof-of-concept demonstration. As before, silver was used for the large area Ohmic contact at the bottom. Light is incident from the side coated with titanium dioxide, however, light absorption in the ultra-thin titanium dioxide layer is expected to be minimal. Most of the light absorption and minority carrier generation should take place in the silicon.

Under AM 1.5 illumination, classic solar cell characteristics are measured. The measured short-circuit current is 19.3 mA/cm^2 (Fig. 3(b)), confirming that the photogenerated electrons can pass through the titanium dioxide layer. It was shown in Fig. 3(c) that without the titanium dioxide interlayer, the Al/p-Si Schottky device has Ohmic current-voltage characteristics, making the structure useless for a solar cell. In contrast, with the titanium dioxide interlayer, the Al/TiO₂/Si heterojunction blocks the holes in silicon from flowing to aluminum (as shown in Fig. 2(a) above). The efficient hole-blocking enables the heterojunction diode to achieve a low dark-current and under illumination yields an open-circuit voltage of 0.52 V (Fig. 3(b)). The fill factor is a respectable 70%, showing that the resistive losses across the thin titanium dioxide layer are also not substantial.

Extrapolating the linear portion of the dark current-voltage characteristics on a semilog plot (Fig. 3(c)), we extract a J_0 of $2 \times 10^{-9} \text{ A/cm}^2$ with an ideality factor (n) of 1.4. Both of these values are much worse than those measured in high-quality p-n junction diodes. One possible explanation for the non-ideality could be the minority carrier recombination at the unpassivated back contact. Experiments to confirm this hypothesis are currently underway.

The peripheries of the devices were not masked during AM1.5 illumination, so it is possible that carriers photogenerated at the periphery of the device may laterally diffuse in silicon to the TiO₂/Si interface, artificially inflating the value of the short-circuit current. However, this does not change our main result: TiO₂/Si heterojunction block holes while allowing electrons to pass through.

In conclusion, we demonstrated a low-temperature processed TiO₂/Si wide bandgap heterojunction on silicon. The structure selectively blocks the transport of holes from silicon to the titanium dioxide layer. AFM images suggest that the ultra-thin titanium dioxide layers are smooth, conformal, and probably amorphous. Surface science studies confirm the existence of titanium dioxide on the surface of silicon. Finally, we show that the heterojunction can be used to separate photogenerated carriers in p-type silicon. The low fabrication temperature of the heterojunction may make it an attractive route towards the fabrication of low-cost, but efficient, crystalline silicon solar cells.

This work was primarily supported by the DOE Sunshot Grant No. DE-EE0005315 and National Science Foundation Grant No. CHE-0924104, and also by the National Science Foundation Princeton MRSEC Grant (DMR-0819860). Gabriel Man acknowledges the Ph.D. fellowship from Natural Sciences and Engineering Research Council of Canada (NSERC). Will McClain acknowledges support from National Science Foundation IGERT: Nanotechnology for Clean Energy (DGE-0903661).

¹J. C. Bean, *Proc. IEEE* **80**, 571 (1992).

²H. Kroemer, *Surf. Sci.* **132**, 543 (1983).

³J. C. Bean, L. C. Feldman, A. T. Fiory, S. Nakahara, and I. K. Robinson, *J. Vac. Sci. Technol. A* **2**, 436 (1984).

⁴J. Pelletier, D. Gervais, and C. Pomot, *J. Appl. Phys.* **55**, 994 (1984).

⁵C. Long, S. A. Ustin, and W. Ho, *J. Appl. Phys.* **86**, 2509 (1999).

⁶C. Martinet, V. Paillard, A. Gagnaire, and J. Joseph, *J. Non-Cryst. Solids* **216**, 77 (1997).

⁷B. S. Richards, J. E. Cotter, and C. B. Honsberg, *Appl. Phys. Lett.* **80**, 1123 (2002).

⁸W. D. Brown and W. W. Grannemann, *Solid-State Electron.* **21**, 837 (1978).

⁹D. Gebeyehu, C. J. Brabec, N. S. Sariciftci, D. Vangeneugden, R. Kiebooms, D. Vanderzande, F. Kienberger, and H. Schindler, *Synth. Met.* **125**, 279 (2001).

¹⁰W. Kern, *J. Electrochem. Soc.* **137**, 1887 (1990).

¹¹T. J. Dennes and J. Schwartz, *J. Am. Chem. Soc.* **131**, 3456 (2009).

¹²T. J. Dennes and J. Schwartz, *ACS Appl. Mater. Interfaces* **1**, 2119 (2009).

¹³R. Methaapanon and S. F. Bent, *J. Phys. Chem. C* **114**, 10498 (2010).

¹⁴U. Diebold, *Surf. Sci. Rep.* **48**, 53 (2003).

¹⁵J. Moulder, W. Stickle, P. Sobol, and K. Bomben, *Handbook of X-ray Photoelectron Spectroscopy* (Physical Electronics, Inc., 1995).

¹⁶P. Y. Huang, C. S. Ruiz-Vargas, A. M. van der Zande, W. S. Whitney, M. P. Levendorf, J. W. Kevek, S. Garg, J. S. Alden, C. J. Hustedt, Y. Zhu, J. Park, P. L. McEuen, and D. A. Muller, *Nature* **469**, 389 (2011).

¹⁷M. Ritala, M. Leskela, L. Niinisto, and P. Haussalo, *Chem. Mater.* **5**(8), 1174 (1993).

¹⁸Y. W. Chung, W. J. Lo, and G. A. Somorjai, *Surf. Sci.* **64**, 588 (1977).

¹⁹H. C. Card, *IEEE Trans. Electron Devices* **23**, 538 (1976).

²⁰H. J. Hovel and J. M. Woodall, *J. Electrochem. Soc.* **120**, 1246 (1973).

²¹M. Tanaka, M. Taguchi, T. Matsuyama, T. Sawada, S. Tsuda, S. Nakano, H. Hanafusa, and Y. Kuwano, *Jpn. J. Appl. Phys., Part 1* **31**, 3518 (1992).

²²S. Avasthi, S. Lee, Y. L. Loo, and J. Sturm, *Adv. Mater.* **23**, 5762 (2011).